Appl. Phys. A (2017) 123:41
DOI 10.1007/s00339-016-0703-6

Applied Physics A
Materials Science & Processing

# Robustness and fragility of photonic bandgap in photonic amorphous diamond structures

**Shigeki Imagawa**[1] · **Keiichi Edagawa**[1]

Received: 3 June 2016 / Accepted: 14 December 2016 / Published online: 20 December 2016


**Abstract** The robustness and fragility of the photonic bandgap (PBG) in disordered or modified photonic amorphous diamond (PAD) structures were investigated via numerical calculations. The original PAD has a rod-connected random network structure with a highly ordered local tetrahedral configuration, and it forms a sizable PBG. Our calculations indicated that the PBG of PAD is relatively robust against the introduction of positional disorder that distorts the local tetrahedral configuration, but considerably fragile against the fragmentation of the network structure. PBG formation in a higher frequency region was found in a PAD structure of isolated dielectric spheres. Based on these findings, the physical origin of PBG formation in PADs has been discussed in light of the picture of dielectric and air bands.

## 1 Introduction

In 1987, Yablonovitch [1] and John [2] proposed the idea that a three-dimensional (3D) photonic band gap (PBG), in which electromagnetic wave propagation is forbidden in all directions, can be realized in artificial periodic dielectric structures, namely photonic crystals. A 3D PBG was predicted to enable 3D light confinement within a volume comparable to the wavelength without substantial loss, which is difficult to achieve with other media. Such strong light confinement is expected to lead to the development of novel types of efficient, minuscule optical devices [3].

✉ Keiichi Edagawa
edagawa@iis.u-tokyo.ac.jp

[1] Institute of Industrial Science, University of Tokyo, Tokyo, Japan

Recently, photonic amorphous materials, i.e., artificial or natural amorphous structures of dielectrics, have gained growing attention [4–19] owing to their peculiar light transport properties and unique features related to isotropic PBG formation, noniridescent structural coloration, etc. With regard to PBG formation, Jin et al. [4] first reported the formation of a 2D PBG for transverse magnetic (TM) polarization in a photonic amorphous structure consisting of dielectric cylinders in 2001. Since then, the formation of 2D TM PBGs has been reported in similar amorphous structures [5, 6]. In general, the Bragg scattering of light due to lattice periodicity is believed to be the main origin of PBG formation in conventional photonic crystals; this should not be the case for photonic amorphous materials, which have no lattice periodicity. Instead, the evanescent coupling of Mie resonances of individual dielectric cylinders has been discussed as a plausible origin of the PBG formation in such photonic amorphous materials [5–7]. Recently, the formation of a sizable "complete" 2D PBG (PBG both for TM and TE polarizations) has been shown to be realizable in some 2D photonic amorphous structures [7].

The formation of a full 3D PBG has recently been demonstrated in a photonic amorphous structure via numerical calculations [16] as well as microwave and terahertz wave transmission experiments [17, 18]. This amorphous structure consists of a random network of dielectric rods with a diamond-like local tetrahedral configuration and is therefore named photonic amorphous diamond (PAD). It has been shown that the 3D PBG in PAD is clean with no trace of localized photonic states within it [17, 19]. This indicates that strong light confinement is realizable in PAD as well as conventional photonic crystals, and it has actually been demonstrated numerically [19].

The physical origin of the PBG formation in PAD remains unclear. As described above, evanescent coupling of Mie resonances is a plausible explanation of the TM-gap formation in 2D photonic amorphous structures of isolated dielectric cylinders. However, such a mechanism appears not to work properly for the PBG formation in PAD that consists of a continuous network structure. In the present work, we modeled disordered or modified PAD structures and investigated the PBG formation in them to clarify the roles of the local order and connectivity of the network structure of PAD in the PBG formation.

## 2 Computational methods

The original PAD structure was constructed from a continuous random network (CRN) model that was originally developed to describe the atomic arrangement of amorphous Si or Ge [20–22]. The PAD structure was constructed by connecting tetrahedral bonds in the CRN structure with dielectric rods, as shown in Fig. 1. More specifically, the CRN structure constructed by Barkema and Mousseau [22] was used, which is characterized by a high degree of local regular-tetrahedron order and by the complete absence of lattice periodicity. This CRN structure, and therefore the PAD structure, consists of a periodic arrangement of cubic supercells with a size of $(11.5d)^3$ ($d$: average bond length). The radius ($r_0$) of the rods was set as $r_0/d = 0.26$, resulting in an air volume fraction of 78%. Detailed descriptions of the design of the original PAD structure have been given in our previous papers [16–18].

We constructed three types of disordered or modified PAD structures: positionally disordered (pd-), fragmented (f-), and dielectric-sphere (ds-) PADs. In pd-PADs, a random positional shift was given to each node of the network of the original PAD. The maximum distance ($s$) of the shift was set as $s/d = 0.1$, 0.2, 0.3, and 0.4. That is, the distance of the shift was randomly chosen within the range [0, $s$], while the direction of the shift was randomly chosen from every $4\pi$ direction. Here, the network topology remains unchanged because $s/d < 0.5$; fourfold connectivity is preserved at every node in the network structure. The radial distribution functions (RDFs) were calculated for the node points in pd-PADs. Here, the RDF is defined as the average point density in the spherical shell ($r$, $r + \mathrm{d}r$) around an arbitrarily selected node point. In f-PADs, we removed the central part with the length ($b$) from every rod, because of which the network was fragmented (Fig. 2). Here, we set $b/d = 0.1$ and 0.2.

Finally, in ds-PADs, we arranged dielectric spheres with the radius ($u$) at the node points of the network of the original PAD. Here, we set $u/d = 0.45$ 0.50, and 0.55, for which the spheres are isolated, in contact, and overlapped, respectively, as shown in Fig. 3. For comparison, crystalline counterparts of ds-PADs, i.e., dielectric-sphere (ds-) photonic crystalline diamonds (PCDs) were also constructed, where we arranged dielectric spheres at the lattice points in the crystalline diamond structure.

The spectral intensities, which represent the photonic density of states (PDOS), and the eigenmodes were calculated using a finite-difference time-domain (FDTD) spectral method originally developed by Chan et al. [23]. In this method, we start from a random electromagnetic field and calculate its time evolution. The time evolutions at each position is then Fourier transformed into the frequency domain to obtain the PDOS and eigenmodes. For pd-, f-, and ds-PAD structures, the calculations were made for a periodic supercell structure of size $(11.5d)^3$. On the other hand, for ds-PCDs, we used a crystalline diamond structure with a fictitious supercell $(5a_0)^3 = (11.5d)^3$, where $a_0 = 4d/\sqrt{3}$ denotes the lattice constant of the crystalline diamond. The use of the fictitious supercell structure for ds-PCDs enables us to compare the results obtained under exactly the same conditions for ds-PADs and ds-PCDs. For the details of the calculation method, we followed Refs., [17, 18]. For ds-PCDs, the photonic band structure was also calculated via a plane-wave expansion method using "BandSOLVE" (RSoft Design Group, Inc.).

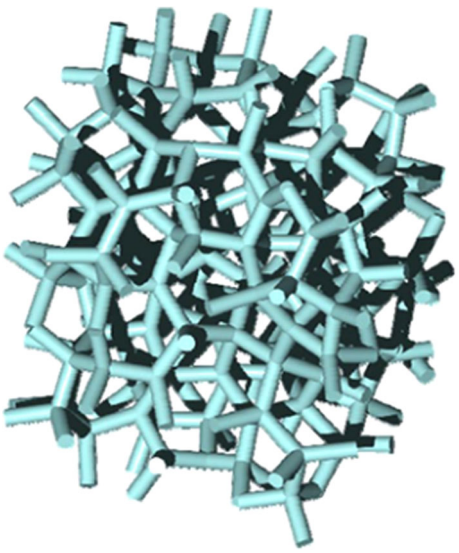

**Fig. 1** Computer graphics image of the original PAD

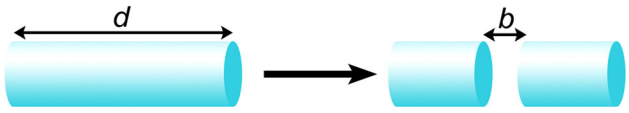


**Fig. 2** Schematic illustration of the construction of f-PADs. The central part with the length ($b$) has been removed from each rod having the length ($d$)

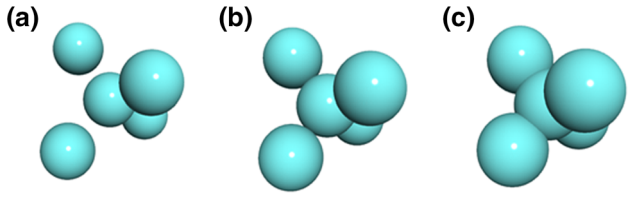


**Fig. 3** Local structures of ds-PADs with $u/d = 0.45$ (**a**), 0.50 (**b**), and 0.55 (**c**), where the spheres are isolated, in contact, and overlapped, respectively

## 3 Results

### 3.1 Positionally disordered PADs

Figure 4 shows the RDFs calculated for the original PAD ($s/d = 0$), and pd-PADs ($s/d = 0.1$, 0.2, 0.3 and 0.4). In the RDF for $s/d = 0$, the first peak at $r = d$ is very sharp with a full width at half maximum (FWHM) value of approximately $0.1d$. This peak represents the bond-length distribution, and its sharpness indicates the presence of a high local order with almost the same lengths for all the bonds. The second peak at $r \approx 1.7d$ is also relatively sharp but the subsequent peaks at $r \approx 2.4d$ and $3d$ are very broad and only marginally observed. Then, no peaks can be detected in the range $r > 3.5d$. This indicates that the original PAD has no order in the range beyond $r \approx 3.5d$. It should be noted that the range $r > 3.5d$ corresponds to $r > 1.5a_0$. This verifies the fact that the original PAD has no trace of the diamond-lattice periodicity.

In Fig. 4, as the value of $s$ increases, i.e., as the degree of disorder increases, the first and second peaks become smaller and broader. For $s/d = 0.3$ and 0.4, they disappear almost completely, indicating the loss of local order.

Figure 5 presents the spectral intensities calculated for the original PAD ($s/d = 0$), and pd-PADs ($s/d = 0.1$, 0.2, 0.3 and 0.4), where the frequency is in units of ($c/a_0$) ($c$: speed of light). In all the calculations, the refractive index of dielectric rods was set as $n = 3.6$. In all the spectra, large decreases in intensity are clearly seen, corresponding to 3D PBGs. The ratios of PBG width ($\Delta f$) to the midgap frequency ($f_c$) were estimated to be $\Delta f/f_c \approx 18.9$, 16.7, 16.2, 15.2, and 13.7% for $s/d = 0$, 0.1, 0.2, 0.3, and 0.4, respectively. It is noteworthy here that sizable 3D PBGs survive even in pd-PADs with $s/d = 0.3$ and 0.4, in which the local order appears to be lost almost completely, as shown in the RDFs in Fig. 4. In addition, the PBG depths at $f_c$ for $s/d = 0.3$ and 0.4 are approximately 80 dB, which is not significantly different from those for the original PAD with $s/d = 0$. From these facts, we can conclude that the PBG is considerably robust against positional disorder that distorts the local tetrahedral configuration in the network PAD structure.

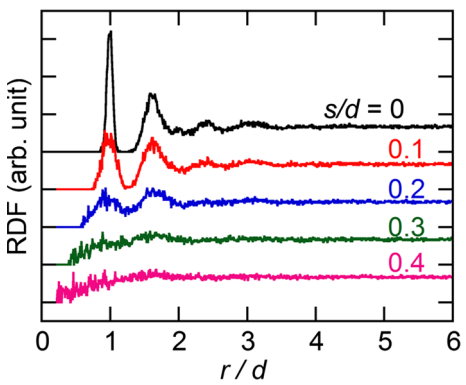


**Fig. 4** Radial distribution functions calculated for the original PAD ($s/d = 0$), and pd-PADs ($s/d = 0.1$, 0.2, 0.3 and 0.4)

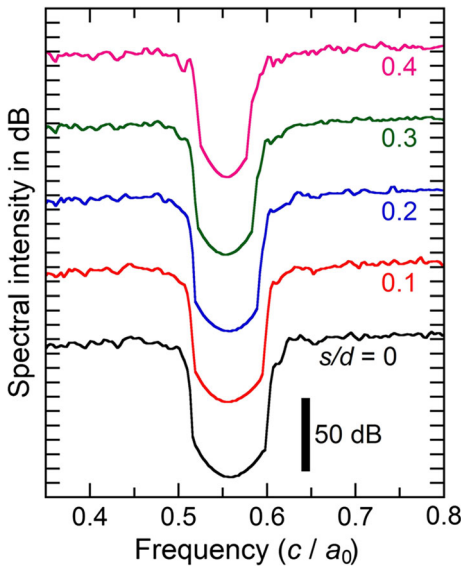


**Fig. 5** Spectral intensities calculated for the original PAD ($s/d = 0$), and pd-PADs ($s/d = 0.1$, 0.2, 0.3 and 0.4)

### 3.2 Fragmented PADs

Figure 6 shows the spectral intensities calculated for f-PADs with $b/d = 0.1$ and 0.2, which are compared with that for the original PAD ($b/d = 0$). Here, the refractive index of dielectric rods was set as $n = 3.6$. In contrast to the results for pd-PADs in Fig. 5, the 3D PBG is drastically reduced in the spectra of f-PADs. In the spectrum for $b/d = 0.1$, a small 3D PBG with $\Delta f/f_c \approx 4.8\%$ can be seen at $f_c \approx 0.64c/a_0$. Here, the upward shift of the PBG position from $f_c \approx 0.56c/a_0$ for the original PAD can be attributed to the decrease in the volume fraction of dielectric parts, which resulted in a decrease in the average refractive index of the structure. In the spectrum of $b/d = 0.2$, no trace of PBG can be detected. These results indicate the considerable fragility of PBG against the fragmentation of the network structure of PAD.

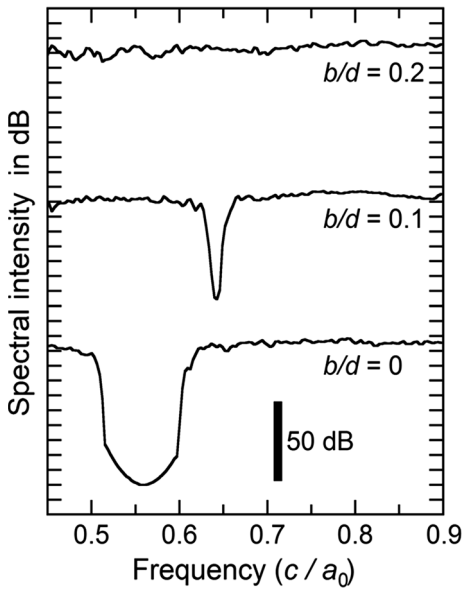


**Fig. 6** Spectral intensities calculated for the original PAD ($b/d = 0$), and f-PADs ($b/d = 0.1$ and 0.2)

### 3.3 Dielectric sphere PADs and PCDs

Figure 7 shows the spectral intensities calculated for ds-PADs (black) and ds-PCDs (blue) with $u/d = 0.45$, 0.50, and 0.55. Here, the refractive index of dielectric rods was set as $n = 4.0$. In the spectra, decreases of intensity by >70 dB are observed, indicating the formations of 3D PBGs. Here, we notice that the PBG positions in ds-PADs are in good agreement with those in the corresponding ds-PCDs. For $u/d = 0.45$, we can observe a large PBG at $f_c \approx 0.72c/a_0$ in each spectrum of ds-PAD and PCD. For $u/d = 0.50$, we have a large PBG at $f_c \approx 0.46c/a_0$, a relatively small one at $f_c \approx 0.65c/a_0$ for ds-PCD, and a small one at $f_c \approx 0.65c/a_0$ for ds-PAD. Finally, for $u/d = 0.55$, a large PBG is observed at $f_c \approx 0.41c/a_0$ for each of the two spectra.

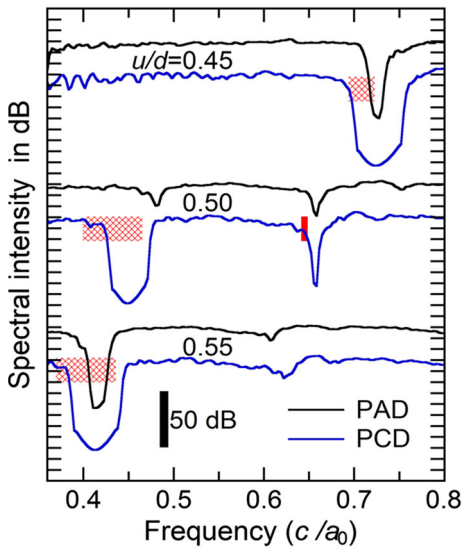


**Fig. 7** Spectral intensities calculated for ds-PADs (*black*) and ds-PCDs (*blue*) with $u/d = 0.45$ 0.50, and 0.55

In Fig. 8a–c, photonic band structures calculated for ds-PCDs with $u/d = 0.45$, 0.50, and 0.55, respectively, are presented, where the red strips indicate the positions of complete 3D PBGs. These frequency ranges are also shown by the red strips in Fig. 7. Here, we have two different types of PBGs: the PBG between the second and third

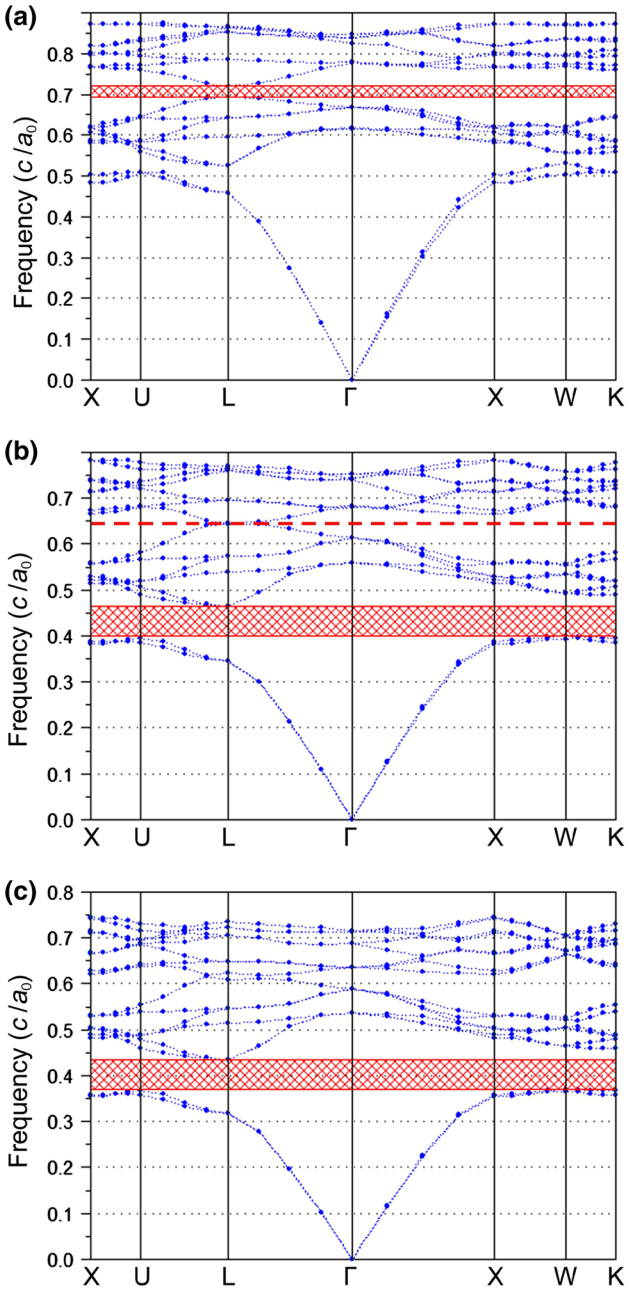


**Fig. 8** Photonic band structures calculated for ds-PCDs with $u/d = 0.45$ (**a**), 0.50 (**b**), and 0.55 (**c**). The positions of complete 3D PBGs are indicated by *red strips*

bands (2–3 gap) and that between the eighth and ninth bands (8–9 gap). For $u/d = 0.55$ in Fig. 8c, we have a large 2–3 gap at $f_c \approx 0.40c/a_0$. For $u/d = 0.50$ in Fig. 8b, a large 2–3 gap is again seen, but its position has shifted slightly upward. Here, an 8–9 gap is on the verge of opening (red broken line); the two bands are barely in contact at the point L. This frequency is indicated by a red vertical line in the corresponding spectrum in Fig. 7, which agrees with the position of the decrease in the spectral intensity. Finally for $u/d = 0.45$ in Fig. 8a, the 2–3 gap is closed, and the 8–9 gap is opened, where the position of the 8–9 gap has shifted slightly upward from the frequency at which the two bands are in contact in Fig. 8b. Here, the slight upward shifts of the 2–3 (8–9) gap positions with decreasing $u/d$ value are attributable to the decrease in the volume fraction of dielectric parts in the structure, which has resulted in a decrease in the average refractive index of the structure.

## 4 Discussion

In previous papers [17, 24], we have discussed the formation mechanism of PBG in PAD. In this section, we first review it.

The physical origin of PBG formation in conventional photonic crystals is often explained in terms of the picture of dielectric and air bands [25]. As an example, let us consider a simple one-dimensional photonic crystal consisting of alternately stacked dielectric and air layers. At the edge of the Brillouin zone at $k = \pi/a$ ($a$: period), the eigenstates are stationary electromagnetic waves with a wavelength of $2a$. We have two ways to position such a wave to conform to the symmetry of the structure: in one way, the maximum points of the electric-field intensity occur in dielectric layers, and in the other, they occur in air layers. The eigenfrequency of the former should be lower than that of the latter, leading to the formation of a PBG.

To examine whether this picture can also be applied to PAD, we previously evaluated the concentration factor (CF) of the electric-field intensity $|E(r)|^2$ in the air region for the eigenstates in the original PAD [17]. Here, CF is defined as

$$\mathrm{CF} \equiv \frac{\int_{V_{\mathrm{air}}} |E(r)|^2 \mathrm{d}r}{\int_{V_{\mathrm{tot}}} |E(r)|^2 \mathrm{d}r}, \tag{1}$$

where $V_{\mathrm{air}}$ and $V_{\mathrm{tot}}$ represent the air volume and total volume, respectively. For comparison, CF has also been evaluated for a rod-connected PCD, which was constructed by connecting tetrahedral bonds in the crystalline structure of diamond with dielectric rods. We set the rod radius as $r_0 = 0.26d$ and the refractive index of rods as $n = 3.0$. The results are reproduced here in Fig. 9. If the electric field is distributed evenly for the dielectric and air regions, CF should equal the volume fraction of the air part, that is, 78%. In Fig. 9, at the lower band top, CF is approximately 65% for both PAD and PCD. As the frequency decreases, CF increases and approaches the air volume fraction of 78%. On the other hand, at the higher band bottom, CF is approximately 93%, which is much higher than the volume fraction value. These results clearly show that the picture of dielectric and air bands can be applied not only to PCD but also to PAD, despite the complete absence of lattice periodicity.

In 3D photonic crystals, the structures in which both dielectric and air regions form connected and percolating networks are known to favor PBG formation [9, 26–28]. The importance of the connected network structure for PBG fomation should be related to the vector nature of electromagnetic fields; in order for the field to be confined in the dielectric or air region to realize a dielectric or air band, a connected network should be favorable to accommodate the continuous field lines [24, 25]. In fact, we have confirmed by examining the eigenstates at the lower band top in our PCD that the continuous field lines are neatly accommodated in the rods connecting nodes in the dielectric network.

Our PAD has such a network structure, which should play a similar role in the realization of dielectric and air bands, leading to PBG formation. This is consistent with the considerable fragility of PBG against the fragmentation of the network structure of PAD shown in Sect. 3.2. When the dielectric network has been segmented, the field lines, which had been accommodated in the network before the segmentation, should be forced to penetrate the air regions. This should increase the eigenfrequency at the lower band top, leading to the closing of the PBG.

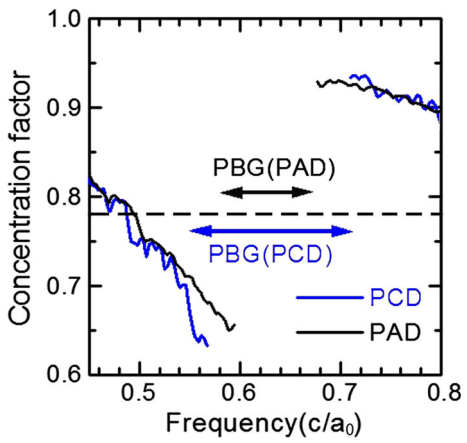


**Fig. 9** Frequency dependences of the concentration factor of the electric field for rod-connected PCD and PAD

The results for pd-PADs in Sect. 3.1 indicate that local structural order is much less important than network connectivity in PBG formation. With the introduction of positional disorder, the local tetrahedral configurations should be distorted. In particular, they should be severely distorted in pd-PADs with $s/d = 0.3$ and 0.4, as evidenced by their RDFs in Fig. 4. Nevertheless, sizable 3D PBGs survive in these structures, exhibiting a high tolerance for the local distortion. This is advantageous for applications because a high precision is not necessary for fabricating a PAD to form a PBG. Here, it should be noted that such pd-PADs keep the fourfold connectivity of the network structure. In previous papers [16, 19], we have shown that a localized state is formed when a rod has been removed from the PAD network structure. Here, the removal of a rod creates two threefold nodes in the network, and a localized state is formed in the space between them. The eigenfrequency of the localized state is located within the PBG. Therefore, such threefold nodes, when introduced in the fourfold network, should close the PBG, if their density is large.

It should be interesting to know what happens if the nodes in the network are entirely threefold or fivefold. Therefore, we constructed threefold and fivefold random network structures and investigated the PBG formation in them. Preliminary results have shown that they exhibit a signature of PBG formation, but the PBGs are much smaller and shallower than those in the PAD with a fourfold network structure. This result indicates the importance of the fourfold connectivity of the network structure in the formation of PBG.

In Sect. 3.3, we presented the results for ds-PADs and ds-PCDs. Here, let us first examine the results for ds-PCDs. In the ds-PCD with $u/d = 0.55$, dielectric spheres are overlapped; dielectric regions are connected to form a network structure. Therefore, this structure resembles a rod-connected PCD, for which photonic band structure calculations have previously been made [17, 26, 28]. The calculations have indicated that the rod-connected PCD forms a large 3D PBG between the second and third bands, which agrees with our result for the ds-PCD with $u/d = 0.55$. For ds-PCDs with $u/d \leq 0.5$, where dielectric spheres are in contact or isolated, calculations have previously been performed by other groups [29–31]. Moroz [31] reported the results for $u/d = 0.50$ and 0.40 with various refractive indices, $n$, of rods. Here, for $u/d = 0.50$ with $n = 4.0$, a 2–3 gap and an 8–9 gap are simultaneously formed, and for $u/d = 0.40$ with n = 4.0, where dielectric spheres are isolated, the 2–3 gap gets closed while the 8–9 gap grows considerably. These results are in agreement with our calculations.

It was shown in Fig. 7 that the PBG positions in ds-PADs agree well with those in the corresponding ds-PCDs. This fact suggests that the origin of the formation of each PBG in ds-PADs should be the same as that of the corresponding PBG in ds-PCDs. That is, the PBG at $f_c \approx 0.41c/a_0$ for the ds-PAD with $u/d = 0.55$ that corresponds to the 2–3 gap for the ds-PCD with $u/d = 0.55$ should originate from the realization of dielectric and air bands due to the fourfold connected network structure. On the other hand, the PBG at $f_c \approx 0.72c/a_0$ for the ds-PAD with $u/d = 0.45$ corresponds to the 8–9 gap for the ds-PCD with $u/d = 0.45$, and the origin of the PBG formation should be different from that for the ds-PAD with $u/d = 0.55$.

To investigate the formation mechanism of PBGs in a high-frequency region in the PAD and PCD structures of isolated dielectric spheres, we evaluated the CF for the ds-PAD and ds-PCD with $u/d = 0.45$, and the results are shown in Fig. 10. For both structures, the tendency of dielectric and air bands is observed: CF values are smaller and larger than the average value of 75% at the lower band top and at the higher band bottom, respectively. In particular, for the PCD of isolated dielectric spheres, the difference between the CF values of the higher band bottom and the lower band top is almost the same as that for the rod-connected network PCD in Fig. 9.

Figure 11a, b shows 2D sections of typical electric-field profiles at around an isolated dielectric sphere for the eigenstates at the lower band top and the higher band bottom, respectively, for the ds-PCD with $u/d = 0.45$. At the lower band top, the electric-field intensity is well concentrated on the dielectric sphere. However, it is not on the entire sphere but only on the outside of the central part. Correspondingly, at the higher band bottom, the electric field is expelled from the region where the field intensity is high at the lower band top. In the high field intensity region at the lower band top in Fig. 11a, the direction of $E$ has been confirmed to be mostly perpendicular to the radial direction of the dielectric sphere. As a result, the field lines

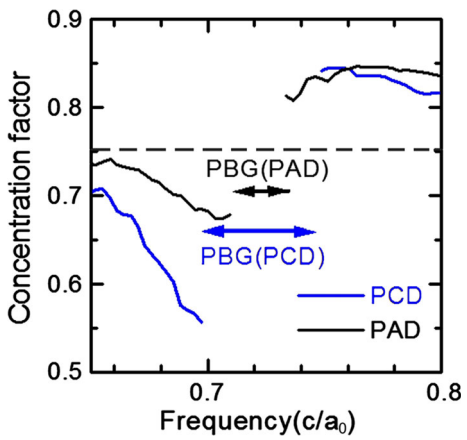


**Fig. 10** Frequency dependences of the concentration factor of the electric field for dielectric sphere PCD and PAD

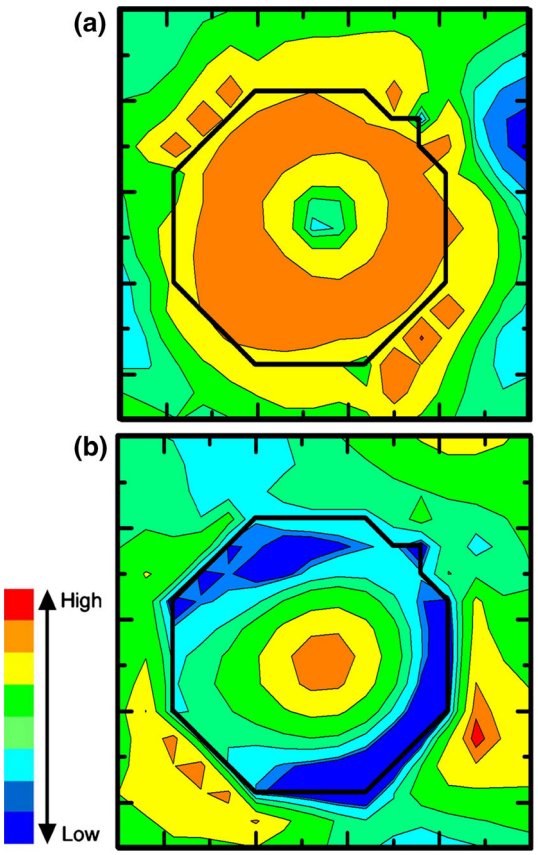


**Fig. 11** 2D sections of typical electric-field profiles around an isolated dielectric sphere for the eigenstates at the lower band top (**a**) and at the higher band bottom (**b**) for the ds-PCD with $u/d = 0.45$

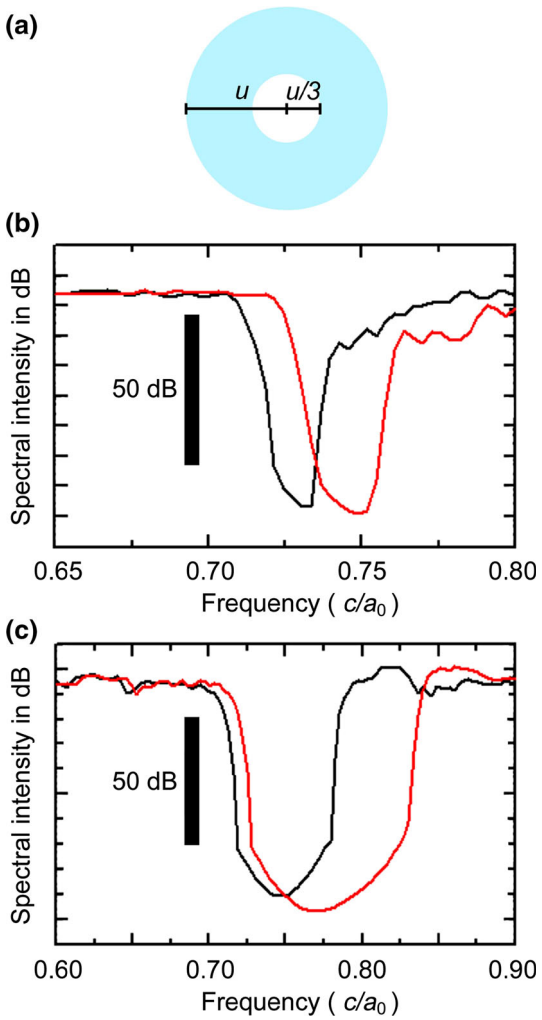


**Fig. 12** **a** Schematic illustration of the hollow dielectric sphere that constitutes hds-PAD and PCDs; **b** spectral intensities calculated for ds-PAD (*black*) and hds-PAD (*red*); **c** those for ds-PCD (*black*) and hds-PCD (*red*). $n = 4.0$ is used for all the calculations

should be mostly closed within the dielectric sphere. This is the reason why the field intensity is well concentrated on the dielectric parts at the lower band top, even in a structure consisting of isolated dielectric parts. This is in sharp contrast to the field pattern at the lower band top in the rod-connected PCD or PAD network, in which the field lines pass along the rods and travel from node to node in the network. Such a difference in the field pattern between the rod-connected and isolated dielectric sphere structures should cause the difference in the PBG position. When the characteristic length of the spatial modulation in the field pattern is long (short), the corresponding frequency should be low (high).

The electric-field patterns in Fig. 11a, b suggest that the CF contrast between the lower band top and the higher band bottom would be enhanced and the PBG would get widened, if the central part of the dielectric sphere is converted to air. To confirm this, we constructed PCD and PAD structures consisting of hollow dielectric spheres (hds-PCD and hds-PAD) and calculated their spectral intensities. Here, the hollow dielectric spheres have an outer radius of $u = 0.45d$ and the inner radius of $u/3$, as shown in Fig. 12a. The spectral intensities calculated for ds- and hds-PADs and those for ds- and hds-PCDs are shown in Fig. 12b, c, respectively. Here, $n = 4.0$ is used for all the calculations. As expected, the PBG sizes have considerably increased: $\Delta f/f_c \approx 5.5$ and 4.7% for hds-PAD and ds-PAD, and $\Delta f/f_c \approx 16.2$ and 11.5% for hds-PCD and ds-PCD, respectively.

## 5 Conclusions

The robustness and fragility of PBG in disordered or modified PAD structures were investigated via numerical calculations. The original PAD has a rod-connected random network structure with a highly ordered local tetrahedral configuration, and it forms a sizable PBG. We constructed three types of disordered or modified PAD structures: positionally disordered (pd-), fragmented (f-),

and dielectric-sphere (ds-) PADs. Photonic density of states calculations for these structures indicated that the PBG of PAD is relatively robust against the introduction of positional disorder that distorts the local tetrahedral configuration, but considerably fragile against the fragmentation of the network structure.

The picture of dielectric and air bands in conventional photonic crystals has been shown to be applicable to the PBG formation in the rod-connected original PAD as well. Here, in the electric-field pattern at the lower band top, the field lines pass along the rods and travel from node to node in the network. This can explain the considerable fragility of PBG against the fragmentation of the network. That is, when the dielectric network has been segmented, the electric-field lines, which had been accommodated in the network before the segmentation, should be forced to penetrate the air regions, increasing the eigenfrequency at the lower band top to close the PBG.

PBG formation in a higher frequency region was observed in a PAD structure of isolated dielectric spheres. The picture of dielectric and air bands is applicable here as well. In this case, the electric-field lines in the field pattern at the lower band top are mostly closed within the dielectric sphere. This is the reason why the field intensity is well concentrated on the dielectric parts at the lower band top, even in a structure consisting of isolated dielectric parts. The difference in the characteristic length of the spatial modulation in the field pattern between the rod-connected and isolated dielectric sphere structures should cause the difference in the PBG position. The PBG was shown to get widened by use of hollow dielectric spheres instead of solid ones.

**Acknowledgements** We thank M. Notomi of NTT Co., Ltd. for valuable comments and discussion. We acknowledge the help of Y. Kamimura in manuscript preparation. This work was supported by a Grant-in-Aid for Scientific Research (B) (24360024) from the Ministry of Education, Culture, Sports, Science and Technology (MEXT).



## References

1. E. Yablonovitch, Phys. Rev. Lett. **58**, 2059 (1987)
2. S. John, Phys. Rev. Lett. **58**, 2486 (1987)
3. M. Notomi, Rep. Prog. Phys. **73**, 096501 (2010)
4. C. Jin, X. Meng, B. Cheng, Z. Li, D. Zhang, Phys. Rev. B **63**, 195107 (2001)
5. H. Miyazaki, M. Hase, H.T. Miyazaki, Y. Kurokawa, N. Shinya, Phys. Rev. B **67**, 235109 (2003)
6. C. Rockstuhl, U. Peschel, F. Lederer, Opt. Lett. **31**, 1741 (2006)
7. M. Florescu, S. Torquato, P.J. Steinhardt, PNAS **106**, 20658 (2009)
8. C. Rockstuhl, F. Lederer, Phys. Rev. B **79**, 132202 (2009)
9. S.F. Liew, J.K. Yang, H. Noh, C.F. Schreck, E.R. Dufresne, C.S. O'Hern, H. Cao, Phys. Rev. A **84**, 063818 (2011)
10. L.F. Rojas-Ochoa, J.M. Mendez-Alcaraz, J.J. Saenz, P. Shurtenberger, F. Scheffold, Phys. Rev. Lett. **93**, 073903 (2004)
11. G.M. Conley, M. Burresi, F. Pratesi, K. Vynck, D.S. Wiersma, Phys. Rev. Lett. **112**, 143901 (2014)
12. L.S. Froufe-Perez, M. Engel, P.F. Damasceno, N. Muller, J. Haberko, S.C. Glotzer, F. Scheffold, Phys. Rev. Lett. **117**, 053902 (2016)
13. J. Sun, B. Bhushan, J. Tong, RSC Adv. **3**, 14862 (2013)
14. Y. Takeoka, J. Mater. Chem. **22**, 23299 (2012)
15. H.W. Yin, B.Q. Dong, X.H. Liu, T.R. Zhan, L. Shi, J. Zi, E. Yablonovitch, Proc. Natl. Acad. Sci. USA **109**, 10798 (2012)
16. K. Edagawa, S. Kanoko, M. Notomi, Phys. Rev. Lett. **100**, 013901 (2008)
17. S. Imagawa, K. Edagawa, K. Morita, T. Niino, Y. Kagawa, M. Notomi, Phys. Rev. B **82**, 115116 (2010)
18. Y. Komiyama, H. Abe, Y. Kamimura, K. Edagawa, Appl. Phys. Lett. **108**, 191110 (2016)
19. S. Imagawa, K. Edagawa, M. Notomi, Appl. Phys. Lett. **100**, 151103 (2012)
20. D.E. Polk, J. Non-Cryst. Solids **5**, 365 (1971)
21. F. Wooten, K. Winer, D. Weaire, Phys. Rev. Lett. **54**, 1392 (1985)
22. G.T. Barkema, N. Mousseau, Phys. Rev. B **62**, 4985 (2000)
23. C.T. Chan, Q.L. Yu, K.M. Ho, Phys. Rev. B **51**, 16635 (1995)
24. K. Edagawa, Sci. Technol. Adv. Mater. **15**, 034805 (2014)
25. J.D. Joannopoulos, S.G. Johnson, J.N. Winn, R.D. Meade, *Photonic Crystals-Molding the Flow of Light* (Princeton University Press, Princeton, NJ, 2008)
26. M. Maldovan, E.L. Thomas, Nat. Mater. **3**, 593 (2004)
27. E.N. Economou, M.M. Sigalas, Phys. Rev. B **48**, 13434 (1993)
28. C.T. Chan, S. Datta, K.M. Ho, C.M. Soukoulis, Phys. Rev. B **50**, 1988 (1994)
29. K.M. Ho, C.T. Chan, C.M. Soukoulis, Phys. Rev. Lett. **65**, 3152–3155 (1990)
30. H.S. Sozuer, J.W. Haus, R. Inguva, Phys. Rev. B **45**, 13962–13972 (1992)
31. A. Moroz, Phys. Rev. B **66**, 115109 (2002)